applied sciences

MDPI

Article

Parallel Continuum Delta: On the Performance Analysis of Flexible Quasi-Translational Robots

Oscar Altuzarra, Mónica Urizar *, Alfonso Hernández and Enrique Amezua

Mechanical Engineering Department, Bilbao School of Engineering, University of the Basque Country (UPV/EHU), Plaza Ingeniero Torres Quevedo 1, 48013 Bilbao, Spain; oscar.altuzarra@ehu.eus (O.A.); a.hernandez@ehu.eus (A.H.); enrique.amezua@ehu.eus (E.A.)

* Correspondence: monica.urizar@ehu.eus

Abstract: In the field of rigid parallel manipulators, the Delta parallel robot is one of the most popular choices in the industry due to its ability to adapt to a wide range of applications, particularly pick-and-place tasks. In this paper, the authors present novel designs of Delta-type continuum parallel manipulators with flexible bars, solving both their direct and inverse kinematics, as well as obtaining the associated workspace. The continuum parallel manipulators, unlike conventional robots, incorporate certain flexible elements, such as slender rods that make up the kinematic chains of the Delta manipulators proposed in this work. As a consequence of the flexibility of these rods, a purely translational movement will not be generated, since it is necessary to analyze the zones of the workspace where a parasitic motion related to the inclination of the moving platform compromises the task devised. In addition, an experimental prototype of the Keops-Delta continuum manipulator has been built, and several experimental tests have been carried out to validate the proposed theoretical model.

Keywords: parallel continuum manipulators; Cosserat rods; parasitic angle; workspace

check for updates

Citation: Altuzarra, O.; Urizar, M.; Hernández, A.; Amezua, E. Parallel Continuum Delta: On the Performance Analysis of Flexible Quasi-Translational Robots. *Appl. Sci.* **2024**, *14*, 9744. https://doi.org/10.3390/app14219744

Academic Editors: Nicola Pio Belfiore and Alessandro Gasparetto

Received: 10 September 2024
Revised: 14 October 2024
Accepted: 22 October 2024
Published: 24 October 2024

Copyright: © 2024 by the authors. Licensee MDPI, Basel, Switzerland. This article is an open access article distributed under the terms and conditions of the Creative Commons Attribution (CC BY) license (https://creativecommons.org/licenses/by/4.0/).

1. Introduction

Parallel Continuum Manipulators (PCMs) are robotic devices that, in general terms, consist of a fixed platform and a moving platform connected by several flexible elements, in a closed-chain morphology typical of parallel kinematics. Unlike conventional robots formed by rigid elements, PCMs use flexible elements such as flexible rods, cables, or springs to connect the rigid end-effector to their actuators [1]. These manipulators offer great versatility as well as flexibility and precision in object manipulation, which makes them ideal for applications in fields such as medicine, aerospace, and especially in robot-human collaborative work, as in the case of the so-called Collaborative Robots, CoBots [2,3]. Indeed, knowing that impact mitigation is a core issue in the field of collaborative robotics, this type of continuum manipulator is gaining special attention, with the aim of developing novel flexible spatial mechanisms, such as the parallel elastic mechanism made of thin plates recently proposed in [4].

PCMs share some characteristics with classical parallel Kinematic machines and compliant mechanisms [5,6], and attempt to combine the best features of both systems. One of the main challenges in the design and control of PCMs is to ensure stability and precision in the movements. Since flexible elements possess a certain elasticity and deformation, the mobility of those mechanisms is produced by kinematic pairs and flexibility of rods alike, and the definition of the robot's degree of freedom is not so clearly established. A common approach in the literature is to use as degrees of freedom the number of actuators needed to keep a pose in equilibrium. Indeed, many of the current PCMs under study are modifications on classical rigid kinematic machines. For example, a broad line of research on hexapod-like flexible manipulators has emerged, solving a variety of problems such as workspace evaluation, real-time position control and elastic analysis [7–12].

In the field of rigid parallel manipulators, the family of translational parallel manipulators is noteworthy. The best known example of this class of robots is the Delta manipulator [13–16]. The main applications of Delta manipulators are pick-and-place operations [17], packaging of small products (cosmetics, pharmaceutical industry, etc.) [18], high precision assembly operations [6], 3D printers [19] and haptic devices [20]. The Delta robot belongs to the family of lower-mobility parallel manipulators that can be defined as closed-loop spatial mechanisms whose end-effector has only three degrees of freedom controlled by actuation on three identical kinematic chains [21]. This type of rigid-body mechanism is subjected to geometrical constraints produced by the arrangement and morphology of the passive kinematic pairs, making it independent of the actuators' values. In some cases, those geometric constraints fix some output parameters, as is the case of the Delta manipulator, which has fixed orientation parameters, resulting in a pure $3D$ translational motion.

The motivation of this research is the development of Continuum parallel Delta manipulators with the ability to be used in manipulation tasks in cooperative scenarios with humans, incorporating this kind of flexible mechanism in collaborative workspaces such as those proposed in the IIDEA project intended for Inclusion and Integration through Collaborative Robotics [22,23]. For reference, we will use as design specifications the characteristics of commercial Delta robots, and specifically the Drylin robot Delta from IGUS Company [24].

Few works can be found on flexible lower-mobility parallel manipulators [25–28]. It is important to note that in these flexible manipulators, it is not possible to impose strict constraints, as in the case of their rigid counterparts, precisely because of the flexibility of the rods. In relation to the continuum Delta, this means that the moving platform can have a varying angle of inclination as it moves, giving rise to the so-called parasitic motions [29,30] and making the analysis of the behaviour of this type of flexible manipulator more difficult [31].

Among the existing methods for modelling manipulators with flexible rods, we will use in this work the Cosserat's theory. Such a model for slender flexible elements has to be coupled with the Dynamic equilibrium of the whole system under all actions, resulting in a nonlinear system of differential equations whose solution can be approached in several ways [7,10,32–35]. Otherwise, discrete multibody and energetic approaches can be applied, as in [36–38].

The aim of this work is to carry out a complete kinematic analysis of the Delta type flexible manipulators that will allow us to analyze the resulting workspace and check which zones have a quasi-translational motion and which ones have, on the contrary, an excessive angle of inclination. The load influence over the workspace will be also assessed. The analysis is quasi-static, but inertial effects could also be included in the analysis by simply adding the inertial force and moment to the total load. This is because the mass of flexible elements is negligible with respect to the total mass of the end-effector; hence, a dynamic analysis could be avoided at the first approximation. In addition, focusing on a specific design of a flexible Delta manipulator, in this case the flexible Keops-Delta, an experimental prototype has been built using bars of Nitinol superelastic material and several tests have been carried out so as to validate the proposed modelling.

The novelties of the work presented are the proposal of a new PCM for quasi-translational motion, the introduction of the notion of parasitic motions in such flexible manipulators, the use of motion ellipsoids in PCMs and the experimental verification of the quasi-static analysis of PCMs.

2. Materials and Methods

In this section, the kinematic analysis applicable to PCMs will be presented, briefly explaining the fundamentals of Cosserat rods' theory. The last part of this section will be focused on Delta-type flexible parallel manipulators.

2.1. Cosserat Rods Deformation Modelling

Before solving the position problem of a mechanism formed by slender flexible elements, it is necessary to have a kinematic model of a single rod, which determines the deformation that it takes when it is subjected to a set of external loads. The Cosserat model is a classical approach to this problem, whose mathematical expression may be different depending on whether the rod is discretized in finite elements [39] or whether the continuous expression of the rod is considered [11], the latter being more accurate. In this work, we consider the simplification for the quasi-static case.

The shape of a deformed rod is defined by a parametric Cartesian curve in space $\mathbf{p}(s) \in \mathbb{R}^3$ that depicts the centroid of each cross-section, and the rotation matrix $\mathbf{R}(s) \in \mathrm{SO}(3)$ expressing the orientation of a local frame attached to the section. The x- and y-axes are placed on the principal cross-section axes, while the z-axis is on the tangent to the deformed rod, see Figure 1. Both position and orientation are functions of a scalar reference arc-length parameter s over the finite interval, $s \in [0, L]$, where L is the length of the rod in the reference configuration. It is assumed that cross-sections remain planar.

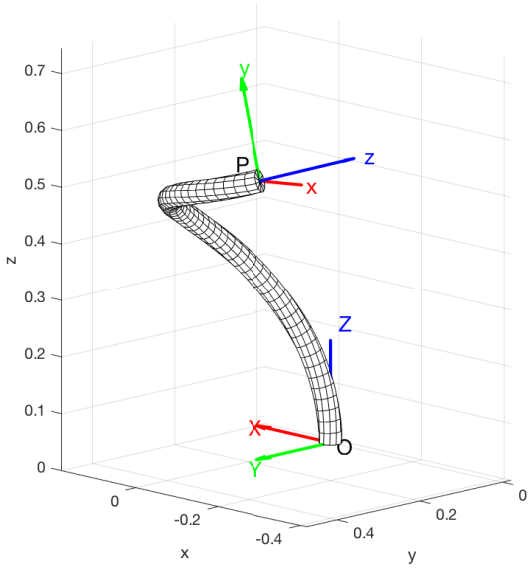

Figure 1. Deformed shape of Cosserat rod.

By differentiating both position and orientation functions with respect to the arc length s, the variables that define the longitudinal deformation $\mathbf{v}$ and the bending deformation $\mathbf{u}$ between cross sections of the bar are obtained:

$$\mathbf{p}' = \mathbf{R}\mathbf{v} \tag{1}$$

$$\mathbf{R}' = \mathbf{R}\hat{\mathbf{u}} \tag{2}$$

where $\hat{\mathbf{u}} = \mathbf{U}(s)$ is a skew-symmetric matrix of the form

$$\mathbf{U}(s) = \begin{bmatrix} 0 & -u_z(s) & u_y(s) \\ u_z(s) & 0 & -u_x(s) \\ -u_y(s) & u_x(s) & 0 \end{bmatrix} \tag{3}$$

The constitutive relationship between strain and stress can be defined depending on the mechanical behaviour of the material. The classical Cosserat rod model assumes that

there is no cross-section deformation, thus the constitutive relationship can be established between the internal forces $\mathbf{n}$ and moments $\mathbf{m}$ and the magnitudes $\Delta\mathbf{v}$ and $\Delta\mathbf{u}$:

$$\mathbf{n} = \mathbf{R}\mathbf{K}_{SE}\Delta\mathbf{v} = \mathbf{R}\mathbf{K}_{SE}(\mathbf{v} - \mathbf{v}_\circ) \tag{4}$$

$$\mathbf{m} = \mathbf{R}\mathbf{K}_{BT}\Delta\mathbf{u} = \mathbf{R}\mathbf{K}_{BT}(\mathbf{u} - \mathbf{u}_\circ) \tag{5}$$

where $\mathbf{v}_\circ$ and $\mathbf{u}_\circ$ are the values at free stress reference condition, and $\mathbf{K}_{SE}$ and $\mathbf{K}_{BT}$ are stiffness matrices for shear-extension and bending-torsion, respectively.

To establish the equations of equilibrium of forces and moments for every infinitesimal piece of the rod ds, internal forces and moments, and applied distributed forces $\mathbf{f}(s)$ and moments $\mathbf{l}(s)$, are considered. So, we get the nonlinear ordinary differential equations describing the evolution of $\mathbf{n}$ and $\mathbf{m}$ along the arc length for the Cosserat rod:

$$\mathbf{n}' + \mathbf{f} = \mathbf{0} \tag{6}$$

$$\mathbf{m}' + \mathbf{p}' \times \mathbf{n} + \mathbf{l} = \mathbf{0} \tag{7}$$

Upon substitution of (4) and (5) into (6) and (7), reordering, and taking into account Equations (1) and (2), a set of differential equations that completely defines the deformed shape for a Cosserat rod model is obtained:

$$\begin{aligned} \mathbf{p}' &= \mathbf{R}\mathbf{v} \\ \mathbf{R}' &= \mathbf{R}\hat{\mathbf{u}} \\ \mathbf{n}' &= -\mathbf{f} \\ \mathbf{m}' &= -\mathbf{p}' \times \mathbf{n} - \mathbf{l} \end{aligned} \tag{8}$$

where

$$\mathbf{v} = \mathbf{K}_{SE}^{-1}\mathbf{R}^T\mathbf{n} + \mathbf{v}_\circ \tag{9}$$

$$\mathbf{u} = \mathbf{K}_{BT}^{-1}\mathbf{R}^T\mathbf{m} + \mathbf{u}_\circ \tag{10}$$

If there are no distributed loads applied to the rod—which usually happens if these flexible rods are implemented in the kinematic chains of parallel manipulators—the rod is straight in its free-stress reference condition. The material properties are constant, and some simplifications can be applied to define the Kirchhoff rod model:

$$\begin{aligned} \mathbf{p}' &= \mathbf{R}\mathbf{e}_3 \\ \mathbf{R}' &= \mathbf{R}\hat{\mathbf{u}} \\ \mathbf{n}' &= \mathbf{0} \\ \mathbf{u}' &= -\mathbf{K}_{BT}^{-1}\left(\hat{\mathbf{u}}\mathbf{K}_{BT}\mathbf{u} + \hat{\mathbf{e}}_3\mathbf{R}^T\mathbf{n}\right) \end{aligned} \tag{11}$$

where $\mathbf{u} = \mathbf{K}_{BT}^{-1}\mathbf{R}^T\mathbf{m}$.

Numeric integration of a system of differential equations in Equation (11) yields the deformed shape of the rod, as well as the evolution of the internal forces and moments along the rod. The solution is approached as a boundary value problem in which some variables are known at $s = 0$ and some others at $s = L$ at the opposite end of the rod. In general, this problem does not have a single solution, and a numeric approach such as a shooting method is required.

For spatial rods, unit quaternions $\tilde{\mathbf{q}} = [q_0\ q_1\ q_2\ q_3]$ are a good option to express the orientation of cross-sections. Thus,

$$\mathbf{R} = \mathbf{I} + \frac{2}{|\tilde{\mathbf{q}}|^2}\begin{bmatrix} -q_2^2 - q_3^2 & q_1q_2 - q_0q_3 & q_1q_3 + q_0q_2 \\ q_1q_2 + q_0q_3 & -q_1^2 - q_3^2 & q_2q_3 - q_0q_1 \\ q_1q_3 - q_0q_2 & q_2q_3 + q_0q_1 & -q_1^2 - q_2^2 \end{bmatrix} \tag{12}$$

Also, we need the derivative of the unit quaternion $\tilde{\mathbf{q}}$ with respect to s, which yields

$$\frac{d\tilde{\mathbf{q}}}{ds} = \frac{1}{2}\tilde{\mathbf{q}}\tilde{\mathbf{u}} = \frac{1}{2}\begin{bmatrix} 0 & -u_x & -u_y & -u_z \\ u_x & 0 & u_z & -u_y \\ u_y & -u_z & 0 & u_x \\ u_z & u_y & -u_x & 0 \end{bmatrix}\begin{Bmatrix} q_0 \\ q_1 \\ q_2 \\ q_3 \end{Bmatrix} \tag{13}$$

Therefore, we have the vector of dependent variables $\mathbf{y} = \{\mathbf{p}\quad \tilde{\mathbf{q}}\quad \mathbf{n}\quad \mathbf{u}\}$ and the non-linear function $\mathbf{f}(s, \mathbf{y})$ from (11), which defines the system of differential equations to be integrated along the independent variable s in $[0,\ L]$, as

$$\frac{d\mathbf{y}}{ds} = \mathbf{f} = \begin{Bmatrix} \mathbf{R}\mathbf{e}_3 \\ \frac{1}{2}\tilde{\mathbf{q}}\tilde{\mathbf{u}} \\ \mathbf{0} \\ -\mathbf{K}_{BT}^{-1}\left((\hat{\mathbf{u}}\mathbf{K}_{BT})\mathbf{u} + \hat{\mathbf{e}}_3\mathbf{R}^T\mathbf{n}\right) \end{Bmatrix} \tag{14}$$

2.2. Analysis of Flexible Manipulators with Cosserat Rods

Let us consider now a parallel mechanism of flexible rods (see Figure 2), where a rigid end-effector is connected to N flexible rods A_iB_i, controlled by some actuators. By attaching a moving frame to the end-effector at reference point $\mathcal{P}$, its orientation can be defined either using a rotation matrix $\mathbf{R}_{EE}$ or a unit quaternion $\tilde{\mathbf{e}}$. The position vector of the rods' attachment-points B_i expressed in the end-effector frame is $\mathbf{r}_i$. The position vector of the rods' proximal-ends A_i expressed in the fixed frame is $\mathbf{a}_i$.

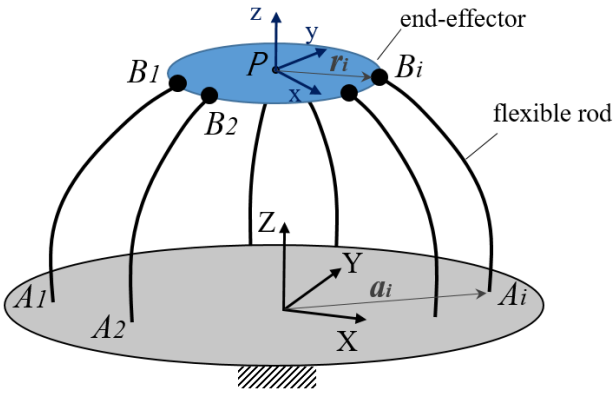

Figure 2. Schematic representation of a general PCM.

Bear in mind that to obtain a feasible pose of the flexible mechanism, there are two conditions that must be satisfied by the deformed shapes of rods: a geometrical assembly with the rigid end-effector, and the static equilibrium of the system.

Regarding the first condition, we have to equate the coordinates of points B_i at the end-effector with those of the distal-ends of the rods. Thus,

$$\mathbf{p}_{\mathcal{P}} + \mathbf{R}_{EE}\mathbf{r}_i = \mathbf{a}_i + \mathbf{p}_i(L_i) \quad i = 1 \ldots N \tag{15}$$

where $\mathbf{p}_i(L_i)$ is the location of the distal-end of the rod from the proximal-end obtained from the deformation model described in Section 2.1.

Also, geometrical conditions depending on how rods' distal ends are joined to the end-effector must be applied. The simplest connection, through spherical joints, makes a null moment appear at the distal-ends. Bearing in mind that $\mathbf{u} = \mathbf{K}_{BT}^{-1}\mathbf{R}^T\mathbf{m}$, we can state the following:

$$\mathbf{u}_i(L_i) = \mathbf{0} \quad i = 1 \dots N \tag{16}$$

Regarding static equilibrium conditions, these are stated for the whole device, which means that the end-effector and all the rods' values are highly coupled in the set of equations. The end-effector is subjected to external load $\mathbf{F}_{ext}$ at $\mathcal{P}$ and $\mathbf{M}_{ext}$, and to reaction forces and moments at B_i attachments due to the rods' deformation, namely $\mathbf{n}_i(L_i)$ and $\mathbf{m}_i(L_i)$, respectively. And so, the following static equilibrium can be stated:

$$\begin{aligned} \sum_{i=1}^{N} \mathbf{n}_i(L_i) - \mathbf{F}_{ext} &= \mathbf{0} \\ \sum_{i=1}^{N} [(\mathbf{a}_i + \mathbf{p}_i(L_i)) \times \mathbf{n}_i(L_i) + \mathbf{m}_i(L_i)] - & \\ -\mathbf{p}_{\mathcal{P}} \times \mathbf{F}_{ext} - \mathbf{M}_{ext} &= \mathbf{0} \end{aligned} \tag{17}$$

In summary, the position problem involves the following equations: the geometric conditions on the position of the distal-ends (15) at each rod; the geometric conditions on the attachment of the distal-ends to the end-effector (16); and the static equilibrium conditions on the end-effector (17), resulting in a total of $6N + 6$ conditions. If the orientation of the end-effector $\mathbf{R}_{EE}$ was expressed with a unit quaternion $\tilde{\mathbf{e}}$, another condition has to be added, namely the unity condition of the quaternion:

$$e_0^2 + e_1^2 + e_2^2 + e_3^2 = 1 \tag{18}$$

This results in a problem with $6N + 7$ conditions.

In the solving process, which follows an iterative numeric approach, a vector of residuals $\mathbf{g}_{res}$ is created with a chosen order to lower the computational cost, namely

$$\mathbf{g}_{res} = \left\{ \begin{array}{c} \mathbf{p}_i(L_i) - \mathbf{p} - \mathbf{R}_{EE}\mathbf{r}_i + \mathbf{a}_i \\ \mathbf{u}_i(L_i) \\ \hline \vdots \\ \hline \sum_{i=1}^{N} \mathbf{n}_i(L_i) - \mathbf{F}_{ext} \\ \sum_{i=1}^{N} [(\mathbf{a}_i + \mathbf{p}_i(L_i)) \times \mathbf{n}_i(L_i) + \mathbf{m}_i(L_i)] - \\ -\mathbf{p}_{\mathcal{P}} \times \mathbf{F}_{ext} - \mathbf{M}_{ext} \\ \hline e_0^2 + e_1^2 + e_2^2 + e_3^2 - 1 \end{array} \right\} \tag{19}$$

Due to the integration involved in each rod, the solution must be approached as a boundary value problem. For each rod, the vector of dependent variables at $s = 0$, $\mathbf{y}_i(0)$, is introduced for integration along L_i with Runge–Kutta. Some of those variables may be known data from boundary conditions while some are guess values for unknowns. While load ($\mathbf{F}_{ext}$, $\mathbf{M}_{ext}$) is considered data, output components ($\mathbf{p}$ and $\tilde{\mathbf{e}}$) can be data or can be guessed, depending on the problem to be solved. A shooting method is applied to verify residuals, and guessed values are updated iteratively until residuals of the boundary conditions are below a tolerance. For that purpose, a Newton method is advisable in which a known starting home-pose helps to initialize the solving of the problem, as those values serve as close guess values to find the proximal solution.

We will be dealing with flexible parallel manipulators where some of the n degrees of freedom of the end-effector, subjected to a given load, can be controlled by n actuators. As an illustrative example, the parallel continuum Keops-Delta manipulator is represented in Figure 3. The three $\underline{P}FFSS$ kinematic chains that form the flexible Keops-Delta are

actuated by three linear guides that control the position of the proximal ends of each rod $\mathbf{p}_i(0) = \mathbf{a}_i(\rho_i)$, which are clamped with a constant vertical orientation given in $\tilde{\mathbf{q}}_i(0) = [1\ 0\ 0\ 0]$. Consequently, three of the output components of the pose of the end-effector will be controlled (*principal* motions, namely $\mathbf{p}_\mathcal{P}$), while the remaining ones, $\tilde{\mathbf{e}}$, will be dependent components of the motion, *parasitic* motions.

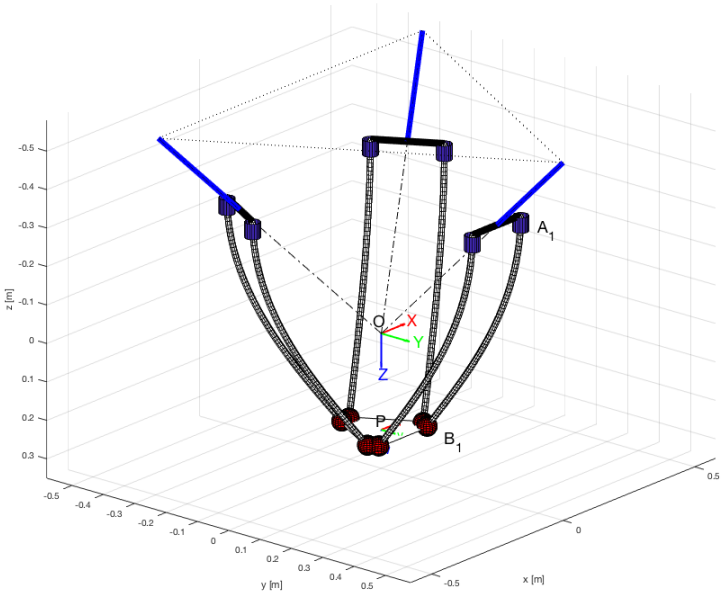

Figure 3. Parallel continuum Keops-Delta 3$\underline{P}FFSS$ with Cosserat Rods.

2.2.1. Forward Kinematics Problem

The Forward Kinematics (FK) consists of determining the pose of the end-effector, i.e, $\mathbf{p}_\mathcal{P}$ the position vector of reference point $\mathcal{P}$, and the orientation given by the unit quaternion $\tilde{\mathbf{e}}$, when input values for each rod ρ_i and a load are imposed. Guess values for unknown variables are required to start a boundary value problem on the vector of residuals in (19), being $\mathbf{u}_i(0)$ and $\mathbf{n}_i(0)$ (6 unknowns per rod) and the output pose, $\mathbf{p}_\mathcal{P}$ and $\tilde{\mathbf{e}}$, a total of 43 unknowns with the system of $6\times6+7=43$ equations in Equation (19).

The Newton method used in the shooting method requires the evaluation of a Jacobian of the residue vector function with respect to the variables of the problem, i.e., the guess values, in order to update them accordingly. A special order for the guess values is considered, so that the guess values associated to a rod are together:

$$\mathbf{h}_{guess} = \left\{ \begin{array}{c} \mathbf{u}_i(0) \\ \mathbf{n}_i \\ \hline \vdots \\ \hline \mathbf{p}_\mathcal{P} \\ \tilde{\mathbf{e}} \end{array} \right\} \tag{20}$$

The Jacobian is then obtained as

$$\mathbf{J}(\mathbf{h}_{guess}) = \frac{\partial \mathbf{g}_{res}(\mathbf{h}_{guess})}{\partial \mathbf{h}_{guess}} \tag{21}$$

The Jacobian related to the Forward Kinematic Problem is a sparse matrix $\mathbf{J} \in \mathbb{R}_{43\times 43}$ of the form

$$\mathbf{J} = \begin{bmatrix} \mathbf{A}_1 & \mathbf{0} & \mathbf{0} & \mathbf{C}_1 & \mathbf{D}_1 \\ \mathbf{0} & \ddots & \mathbf{0} & \vdots & \vdots \\ \mathbf{0} & \mathbf{0} & \mathbf{A}_6 & \mathbf{C}_6 & \mathbf{D}_6 \\ \mathbf{B}_1 & \dots & \mathbf{B}_6 & \mathbf{C} & \mathbf{0} \\ \mathbf{0} & \mathbf{0} & \mathbf{0} & \mathbf{0} & \mathbf{D} \end{bmatrix} \tag{22}$$

Each sub-matrix $\mathbf{A}_i \in \mathbb{R}_{6\times 6}$ is calculated considering the residue associated to the geometric conditions for the rod i and the kinematic variables used as guess values for the rod i. Similarly, matrix $\mathbf{B}_i \in \mathbb{R}_{6\times 6}$ is defined considering the residue associated to the static conditions that affect the whole mechanism and the kinematic variables used as guess values for rod i. Matrix $\mathbf{C}_i \in \mathbb{R}_{6\times 3}$ is calculated considering the residue associated to the geometric conditions for the rod i and the coordinates of $\mathcal{P}$ used as guess values. Matrix $\mathbf{D}_i \in \mathbb{R}_{6\times 4}$ is calculated considering the residue associated to the geometric conditions for the rod i and the kinematic variables used as guess values for the orientation of the end-effector. Finally, matrix $\mathbf{C} \in \mathbb{R}_{6\times 3}$ is defined considering the residue associated to the static conditions and the output position of $\mathcal{P}$ of the end-effector; while matrix $\mathbf{D} \in \mathbb{R}_{1\times 4}$ is defined considering the residue associated to the quaternion normalization condition and the orientation of the end-effector.

After each iteration j, guess values are updated with

$$\mathbf{h}_{guess}^{j+1} = \mathbf{h}_{guess}^{j} - \mathbf{J}^{-1}\mathbf{g}_{res}^{j} \tag{23}$$

and the process starts again until $\mathbf{g}_{res}$ is below a given tolerance.

2.2.2. Translational and Rotational Ellipsoids

As observed in the *FK*, output components are obtained without distinguishing between whether *principal* (controlled) and *parasitic* components. However, for the Inverse Kinematics (IK) it is essential to assess appropriately which components are *principal* and *parasitic*. This is because in these parallel continuum manipulators, there are no hard geometrical constraints among them, as there are in rigid link parallel manipulators [31]. In order to do a proper choice of the type of output variables, it is convenient to evaluate the relative magnitude of the output variables' change under an input increment and detect which are the most feasible motions. For a regular pose, using the FK problem with the input set $\Delta\boldsymbol{\rho}$, the following linearization can be obtained:

$$\begin{Bmatrix} \Delta\mathbf{p}_{\mathcal{P}} \\ \Delta\tilde{\mathbf{e}} \end{Bmatrix} = \begin{bmatrix} \mathbf{J}_T \\ \mathbf{J}_R \end{bmatrix} \Delta\boldsymbol{\rho} \tag{24}$$

where $\mathbf{J}_T$ and $\mathbf{J}_R$ are analogous to translational and rotational Jacobians in velocity analysis of rigid-link mechanisms. From these Jacobians, the principal motions can be obtained.

In a 3 degrees of freedom mechanism like the flexible Keops-Delta 3$\underline{P}FFSS$ under study, the translational Jacobian $\mathbf{J}_T \in \mathbb{R}_{3\times 3}$ can be used to obtain an ellipsoid that shows the three possible translational motions, as shown in Figure 4a. Similarly, for the rotation, $\mathbf{J}_R$ can be used to get the rotational ellipsoid, depicted in Figure 4b, which clearly shows the predominant directions of rotation with respect to the X and Y axes, the rotation with respect to the vertical axis Z being almost zero.

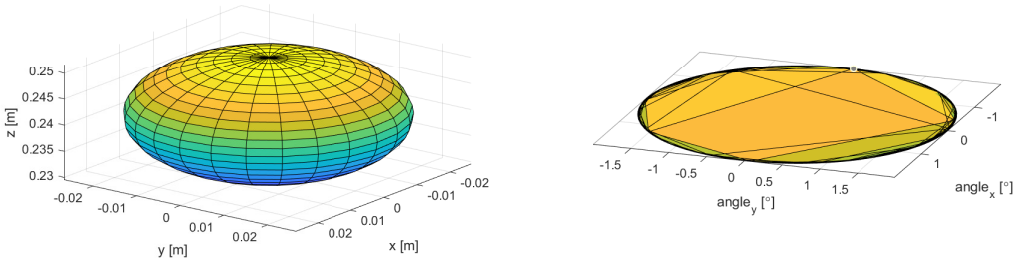

(**a**) (**b**)

Figure 4. (**a**) Translational and (**b**) rotational ellipsoids of flexible Keops-Delta 3$\underline{P}FFSS$.

2.2.3. Inverse Kinematics Problem

Solving the Inverse Kinematics (IK) implies obtaining the input values of actuators $\boldsymbol{\rho}$, for a given load and desired output pose. As mentioned, in these flexible mechanisms, the components of the output pose $(\mathbf{p}_{\mathcal{P}}, \tilde{\mathbf{e}})$ are not all independent output variables, and only principal components $\mathbf{p}_{\mathcal{P}}$ are to be imposed. The rest of the output components, the *parasitic* ones $\tilde{\mathbf{e}}$, are unknowns of the problem and thus require guess values for the procedure to run.

Thus, the variables of the IK problem are

$$\mathbf{h}_{guess} = \left\{ \begin{array}{c} \mathbf{u}_i(0) \\ \mathbf{n}_i \\ \hline \boldsymbol{\rho} \\ \tilde{\mathbf{e}} \end{array} \right\} \tag{25}$$

The Jacobian related to the IK is a sparse matrix $\mathbf{J} \in \mathbb{R}_{43\times 43}$ similar to that of the FK problem:

$$\mathbf{J} = \begin{bmatrix} \mathbf{A}_1 & \mathbf{0} & \mathbf{0} & \mathbf{E}_1 & \mathbf{F}_1 \\ \mathbf{0} & \ddots & \mathbf{0} & \vdots & \vdots \\ \mathbf{0} & \mathbf{0} & \mathbf{A}_6 & \mathbf{E}_6 & \mathbf{F}_6 \\ \mathbf{B}_1 & \dots & \mathbf{B}_6 & \mathbf{E} & \mathbf{F} \\ \mathbf{0} & \mathbf{0} & \mathbf{0} & \mathbf{0} & \mathbf{G} \end{bmatrix} \tag{26}$$

where $\mathbf{E}_i \in \mathbb{R}_{6\times 3}$, $\mathbf{F}_i \in \mathbb{R}_{6\times 4}$, $\mathbf{E} \in \mathbb{R}_{6\times 3}$, $\mathbf{F} \in \mathbb{R}_{6\times 4}$ and $\mathbf{G} \in \mathbb{R}_{1\times 4}$ are defined analogous to the Forward Jacobian.

2.3. Delta-Type Flexible Parallel Manipulators

One of the most successful designs of a Lower Mobility Parallel mechanism is the family of translational parallel mechanisms called Delta [40]. An articulated parallelogram is used in each of the three limbs to introduce a constraint on the rotation of the end-effector about the normal to the parallelogram's plane. This generates a coupled restriction of the three possible rotations, allowing a pure translational motion of the end-effector. A short side of the parallelogram is attached to the end-effector while the other side is translated with an actuator of a variety of types, configuring a family of machines, namely, vertical or horizontal Delta, Keops-Delta and rotational Delta.

In order to design a flexible alternative to those rigid counterpart translational mechanisms, we have to bear in mind that a *hard* geometric constraint is not possible in such a flexible device. By introducing flexible parallelograms, such as those in the Delta-types parallel continuum manipulators in Figures 3 and 5, the motion of the end-effector is not fully restricted, allowing for rotations due to the flexibility of the rods, as shown with the

rotational ellipsoid in Figure 4b. It is therefore relevant to analyze the workspace of these manipulators to check which zones show an optimal quasi−translational behaviour.

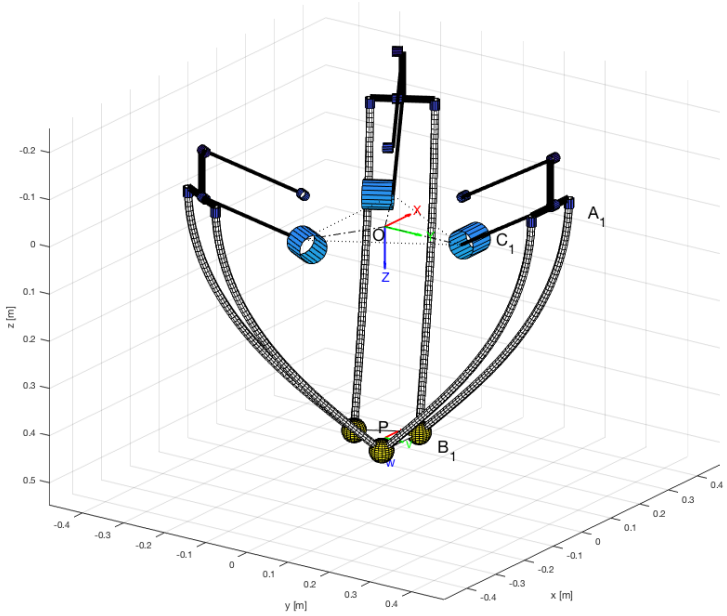

Figure 5. Parallel continuum rotational Delta.

The Keops-Delta, shown in Figure 3, and other designs known as vertical or horizontal Delta are quite similar. The only difference between them lies in the whether the linear actuators are arranged in a vertical or horizontal direction, in the cases of the vertical or horizontal Delta, and in a pyramidal arrangement in the Keops-Delta. Thus, their kinematic analysis is the same, but they differ only in the geometrical arrangement of their linear guides. Another version that was analyzed is the rotational Delta, shown in Figure 5, in which the actuators are rotary motors. A rigid hinged parallelogram is inserted between the motor and the clamping element for the elastic rods' proximal-ends A_i, so that this one performs a circular trajectory, which remains parallel to the fixed horizontal plane at all times.

The flexible parallelogram in each kinematic chain is formed by two Cosserat flexible rods that are attached to the end-effector by spherical joints at their distal-ends B_i, while the proximal-ends A_i are clamped to the actuated element with clamping orientation to be kept in a vertical direction.

For the aforementioned Delta types, the direct and inverse kinematic problems, respectively, are solved as explained next.

2.3.1. Forward Kinematics

The location of the proximal ends of each rod $\mathbf{p}_i(0) = \mathbf{a}_i$ is defined with the three actuators' inputs; the clamping is vertical $\tilde{\mathbf{q}}_i(0) = [1\ 0\ 0\ 0]$; guess values for $\mathbf{u}_i(0)$, $\mathbf{n}_i(0)$ are taken from the previous known pose, as well as those previous pose parameters $\mathbf{p}_\mathcal{P}$ and $\tilde{\mathbf{e}}$; a load is defined, and the numerical minimization of residuals is performed with the guess vector in (20) and the Jacobian (22). Iteratively, we ultimately obtain the end-effector's pose ($\mathbf{p}_\mathcal{P}$, $\tilde{\mathbf{e}}$) and the rods' deformed shape.

2.3.2. Inverse Kinematics

As the principal motions are those that generate a translational motion in the moving platform, $\mathbf{p}_\mathcal{P}$ is given as inputs, and unknown parasitic variables will be those associated with the platform's orientation, $\tilde{\mathbf{e}}$. Therefore, for the inverse kinematics the Jacobian obtained in Equation (25) is needed, together with the following guess vector Equation (25).

3. Results

In this section, the results according to the characterization of the workspace of continuum Delta manipulators will be shown. Moreover, the prototype of the flexible Keops-Delta will be presented, analyzing the results derived from the experimental tests.

3.1. Workspace Analysis of Parallel Continuum Delta Robots

We will focus on the obtaining and analysis of the workspace of the parallel continuum Delta-type robots. In particular, the workspace of the rotational Delta and the Keops-Delta will be determined. Bear in mind that the vertical or horizontal Delta robots are quite similar to the Keops-Delta, differing only in the configuration of the linear actuators.

The strategy followed to obtain the workspace of the flexible Delta manipulators is based on the discretization of this space and on a "wavefront" analysis in such a way that starting from a specific point, adjacent points are analyzed consecutively. To do this, initially, the workspace is divided into a series of k planes associated with a constant Z_k value, this coordinate representing the height of the centroid of the end-effector or moving platform; subsequently, for each of these planes, and starting from the central position $x = y = 0$ of the moving platform, the IK problem of each "neighbouring" point is solved, advancing on a wavefront towards increasing x, y values. When the advancement algorithm detects a singularity [41,42], it will stop at that point and will try on the adjacent ones, so that the boundary of the workspace is delimited. In a last phase, the 3D space is formed with the set of the analyzed Z_k planes. Since the singularities delimit the advance of the wavefront, the spaces we obtain correspond to the so-called *aspects* of the total workspace, i.e., workspaces that are completely free of any type of singularities.

It is worth mentioning that for each point that is solved, not only the value of the associated inputs is obtained (remember that we are solving the IK) but that, since all the kinematic parameters associated with that pose are known, the direct and inverse kinematic Jacobians are also obtained numerically, as well as other relevant parameters such as the value of the parasitic angle, the latter being the angle of inclination of the moving platform about the Euler pole obtained from the $\tilde{\mathbf{e}}$ quaternion. It is of special interest to assess this parasitic angle, since one of the objectives is precisely to be able to extract the zones of the workspace in which this angle is the smallest possible, thus ensuring a quasi-translational motion in this part of the workspace.

Figure 6 shows the workspace corresponding to the Delta rotational flexible manipulator. On the one hand, in Figure 6a, we can see the workspace resulting from imposing a limitation on the actuation system, given in this case by the rotational motors and the range of motion allowed by the articulated parallelogram connecting the motors to the clamping element of the proximal points A_i. The colour scale is based on the value of the parasitic angle of the moving platform, the zones in red being the ones associated with the lowest values. On the other hand, by restricting the maximum parasitic angle to 10°, the practical operational workspace of the flexible rotational delta is obtained in Figure 6b. It can be seen how it constitutes a fairly cylindrical workspace, whose central zone has very small values of the parasite angle (even less than 5° if we keep within a radius of action of 0.2 m), while the peripheral zones have a greater angle of inclination, reaching 10° in the blue extremes.

Regarding the flexible Keops-Delta robot, the corresponding workspace is shown in Figure 7. As before, the resultant workspace, constrained by the limitations of the actuators, is depicted in Figure 7a. In this case, as it will be explained in the next section, the limitation of the actuators is given by the maximum stroke allowed by the linear guides implemented in the prototype, which is 0.6 m. On the other hand, Figure 7b shows the cylindrical-shaped workspace that is obtained when the parasitic angle is limited to 10°. Similar to the rotational Delta, a large central zone ensures parasite angle values of less than 5°. Therefore, we can ensure that the manipulator in this zone has a quasi-translational motion.

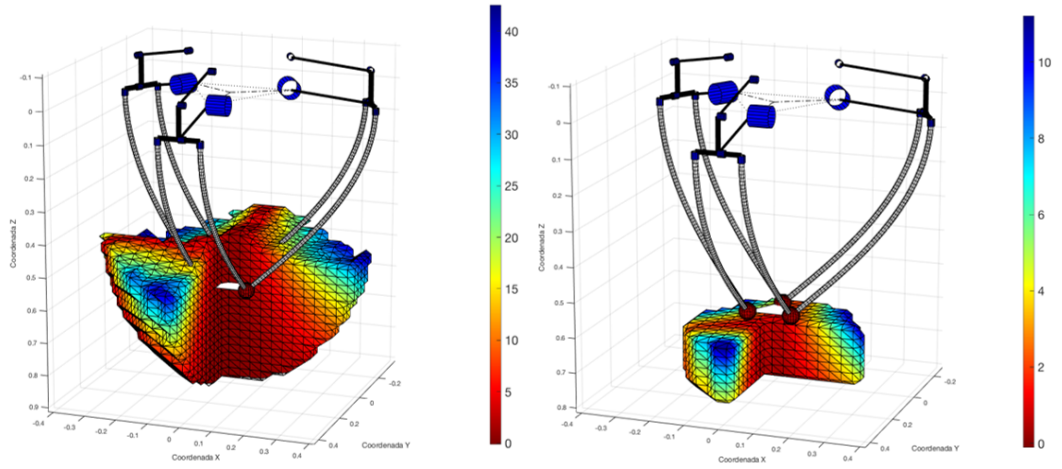

(**a**) (**b**)

Figure 6. Workspace of flexible rotational Delta: imposing limitation on (**a**) actuators and (**b**) parasitic angle.

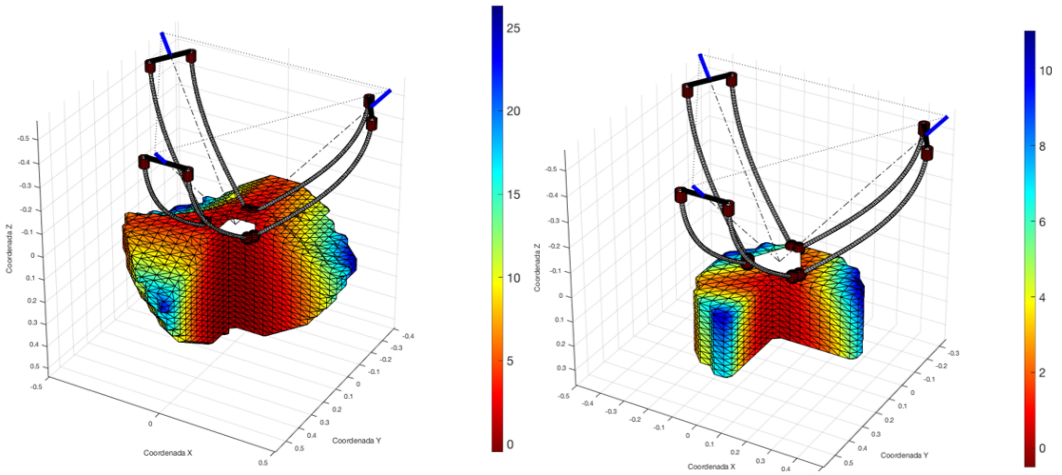

(**a**) (**b**)

Figure 7. Workspace of flexible Keops-Delta: imposing limitation on (**a**) actuators and (**b**) parasitic angle.

Load Influence on the Workspace

Until now, the workspace has been obtained without considering any external load on the end-effector. Next, we analyze different load cases, showing that indeed, it has a great influence on the workspace shape, and also on the distribution of the parasitic angle.

The resultant workspaces associated with different load cases are depicted in Figure 8. On the one hand, the two upper plots, those of Figures 8a and 8b, correspond to an external vertical load $\mathbf{F}_z = 10$ N and $\mathbf{F}_z = 50$ N, respectively. Bear in mind that this load is applied to the centroid of the moving platform. Comparing both cases, it can be observed that the distribution of the parasitic angle remains similar, having a central zone with a low value (around 5°, depicted in green), while the angle increases when approaching the peripheral zones. This performance is the same as the one we had when no external load was applied. However, it can be seen that its size is reduced in some parts of the periphery as the load increases, although it practically does not affect the central part where the quasi-translational behavior is present. In the equivalent rigid Delta manipulators, the maximum load is approximately 5 kg, and we can observe that this flexible Delta manipulator can also support this load, corresponding to the case in Figure 8b with load of $\mathbf{F}_z = 50$ N.

On the other hand, the behavior changes significantly when the load is applied in X or Y directions. For example, Figure 8c shows the case where a load of $\mathbf{F}_y = 10$ N is applied.

It can be seen how the green optimal zone having a low angle of inclination is reduced to a small part of the workspace, while the values in the rest of the zones are very high. In addition, the shape of the workspace also varies greatly, with internal gaps appearing. It makes sense that applying a load in either the X or Y direction is not the most appropriate situation, since it implies that the platform is already starting from a tilted position. In fact, if we compare with the last case (see Figure 8d), in which a load in X-axis is combined with a vertical load, $\mathbf{F}_x = 10$ N and $\mathbf{F}_z = 50$ N, respectively, an orientation of the end-effector closer to the horizontal plane is achieved. Therefore, the workspace returns to a more appropriate shape, although its size is reduced in some of the external parts.

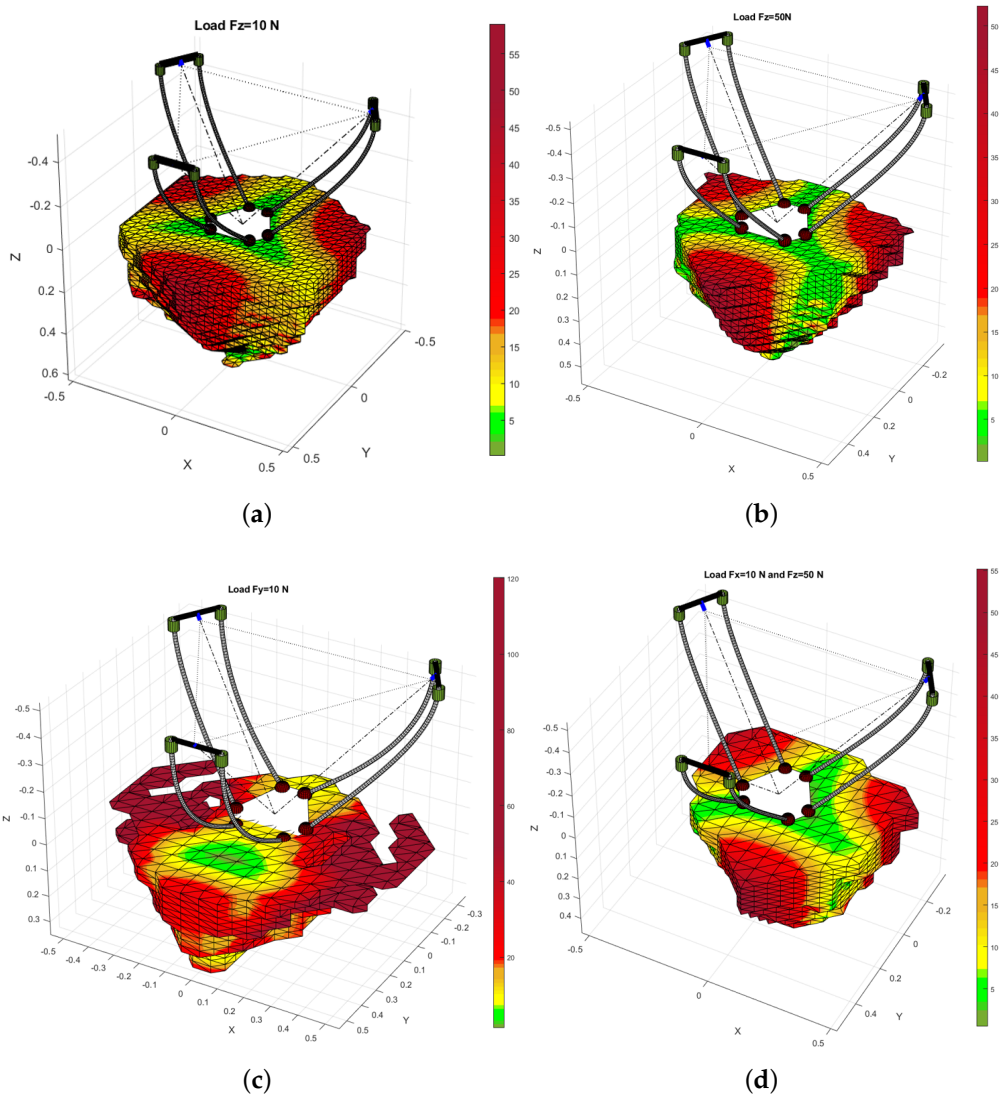

Figure 8. Load influence on workspace of flexible Keops-Delta: (**a**) $\mathbf{F}_z = 10$ N; (**b**) $\mathbf{F}_z = 50$ N; (**c**) $\mathbf{F}_y = 10$ N; (**d**) $\mathbf{F}_x = 10$ N and $\mathbf{F}_z = 50$ N.

3.2. Experimental Validation of the Keops-Delta Prototype

Figure 9 shows the experimental prototype of the parallel continuum Keops-Delta that has been built to perform experimental tests. The flexible rods that make up each of the parallelograms are Nitinol elastic rods of length 0.7 m, with the proximal ends vertically clamped to the linear tables (see detail in Figure 10a), and the distal-ends connected to the spherical joints located on the mobile platform by means of some 3D printed auxiliary pieces (see Figure 10b).

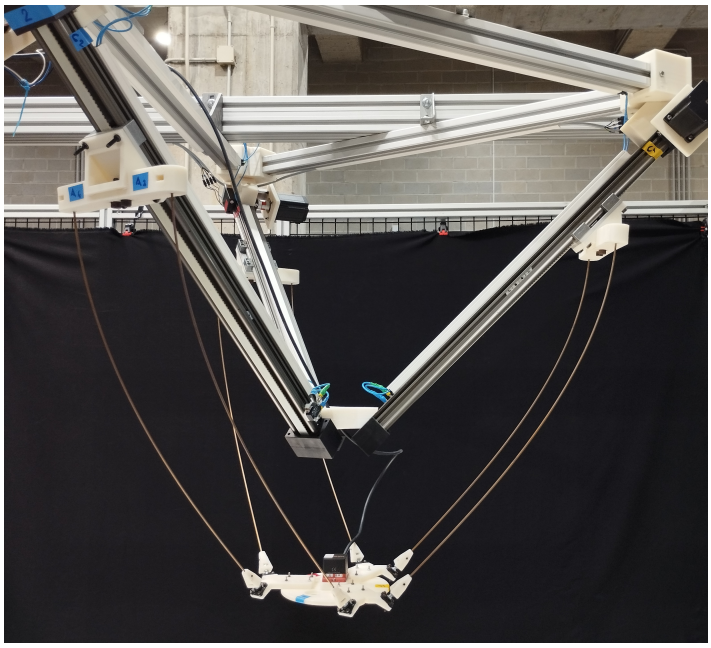

Figure 9. Experimental prototype of parallel continuum Keops-Delta robot.

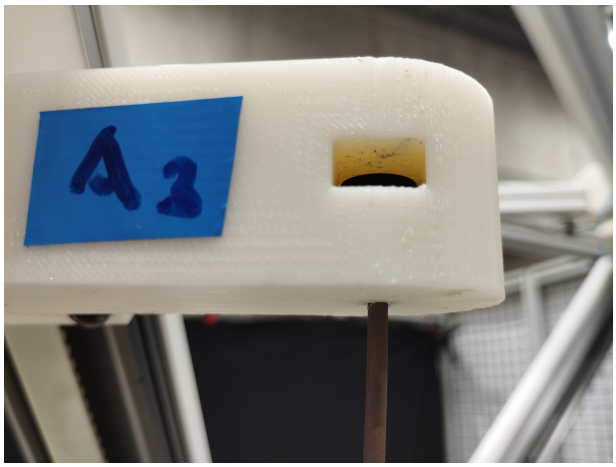

(**a**)

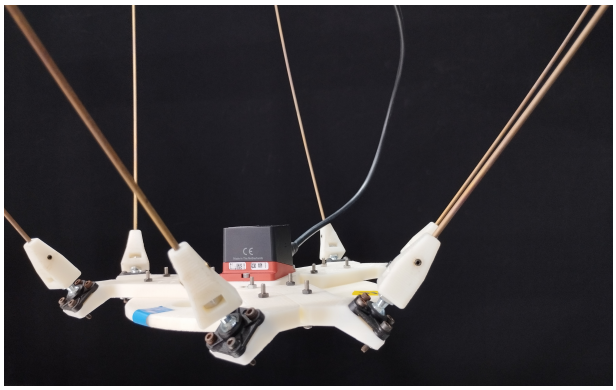

(**b**)

Figure 10. (**a**) Flexible rod clamped to the linear guide; (**b**) Connection to the moving platform through spherical joints.

The prototype combines commercial elements and parts of our own design, which have been 3D printed in our laboratory. The main commercial elements are the aforementioned Nitinol rods of 0.7 m and the following elements from Igus: drylin ZLW linear guides of 0.6 m stroke, stepper motors NEMA23XL and GFSM-AG spherical joints.

For the experimental testing, we have built a graphical user interface (GUI) using App Designer in MATLAB R2023b , as shown in Figure 11. Among all the tasks that have been programmed, the main ones are as follows: the user can move the robot either by giving the values of the linear guides (that is, FK solving), or by establishing the coordinates of the moving platform's centroid (IK solving); also, any predefined trajectory can be directly uploaded to the GUI, and performed; the evolution of main parameters along a certain specified motion can be visualized, such as graphics showing each ρ_i, trajectory of the moving platform, quaternions' values, parasitic orientation Euler angle, and so on.

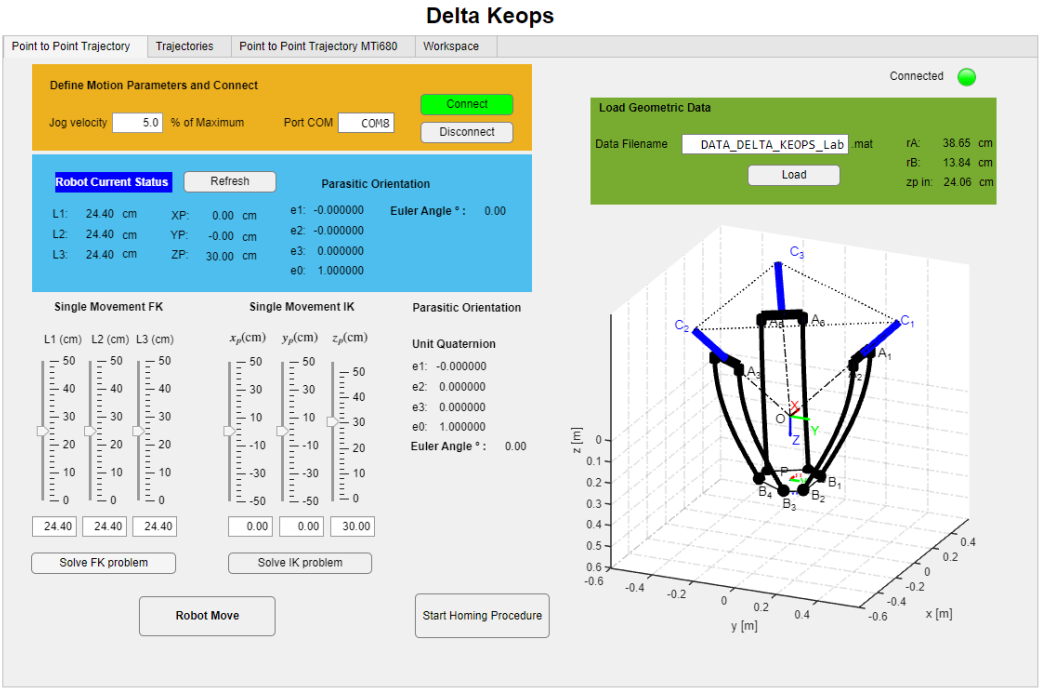

Figure 11. Graphical user interface in App Designer.

To compare the theoretical results from the MATLAB code with the experimentally obtained results, an MTi-680 sensor from Xsens/Movella (Henderson, NV, USA), has been installed at the center of the moving platform to measure inclination, as shown in Figure 10b. Subsequently, the experimental tests that have been carried out will be explained. The motors we used in these tests limit the velocity to 1.17 m/s with a torque of 0.5 Nm, and 0.12 m/s with the maximum torque of 3.1 Nm. Our maximum speed in the tests was 0.1 m/s, but its effect is under study and the velocity can be modified. In Figures 12–14, the theoretical results are plotted in red and the experimental sensed ones are depicted in blue.

The first test consists in performing a vertical motion along the z-axis maintaining null the x and y coordinates of the centroid of the platform. The theoretical and experimental results associated with the quaternions and the corresponding Euler angle, which establishes the inclination of the moving platform with respect to the horizontal plane, can be seen in Figure 12.

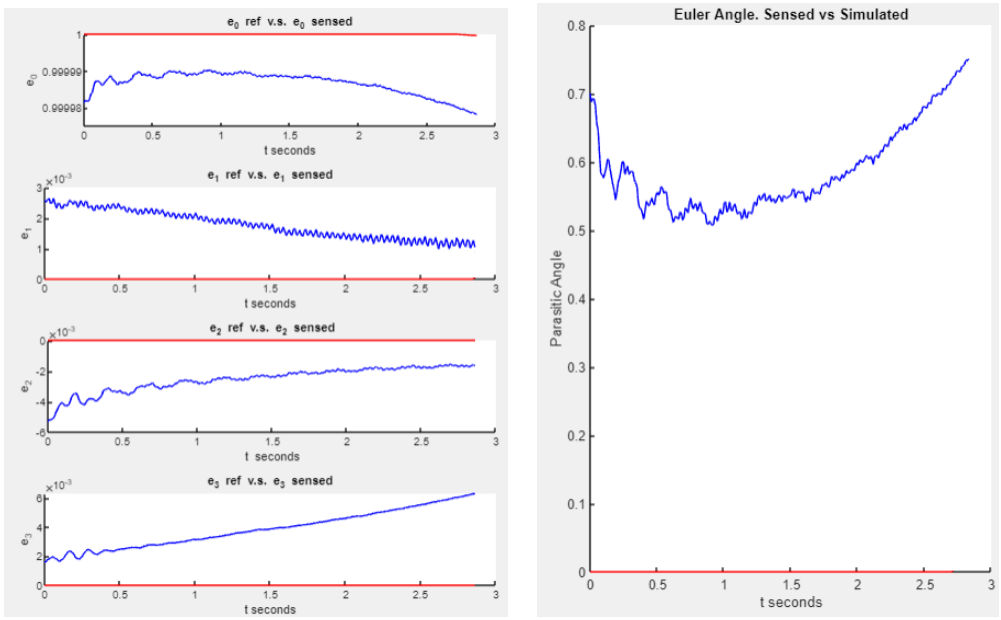

(**a**) (**b**)

Figure 12. Vertical Motion: Theoretical (red) vs. Sensed (blue); (**a**) Quaternions; (**b**) Euler angle.

Figure 12a shows the comparison among the theoretical values of the quaternions (plotted in red) and the real sensed ones (depicted in blue). The three e_i quaternion components, with $i = 1, 2, 3$, represent the rotation around X, Y and Z axes, respectively. As a vertical motion along the Z-axis produces a pure translational motion of the moving platform, in the kinematic model the theoretical values are 0 for the three e_i quaternions, along a value $e_0 = 1$. In the experimental test, the real sensed quaternion components are not exactly zero, the blue curves showing a certain small variation. However, take note that the order of magnitude in the results is 10^{-3}. Figure 12b represents the Euler angle corresponding to those quaternions. As expected, the real sensed value (in blue) is not exactly zero, but the resultant error varies in the approximate range $(0.5°, 0.75°)$.

The discrepancy between the results obtained experimentally and the theoretical values is due to tolerances in the assembly process, as well as the effect of the sensor itself on the moving platform, since the 3D printing platform is very light and the sensor adds weight in the central part. On the other hand, the small oscillations seen in the experimental curves may be related to the vibrations produced in the movement of the manipulator due to the flexibility of the Nitinol rods. Operating at low speed, these vibrations are minimized, while they increase considerably if the robot moves at high speed.

The performance of the manipulator when moving along X and Y axes has also been tested, the resulting graphics being shown in the figures from Figure 13a to Figure 14b. Similarly to the results derived from the vertical testing, small differences exist among the theoretical values and the real sensed ones. Nevertheless, as it can be observed, both in the figures corresponding to the quaternions (Figures 13a and 14a) and the ones corresponding to the Euler angle (Figures 13b and 14b), the theoretical and experimental curves follow exactly the same trend.

In the figures showing the evolution of the inclination angle of the end-effector (Figures 13b and 14b), it can be observed how in the central zone of the curves, corresponding to the end-effector moving along the central areas of the workspace, the angle of inclination presents the minimum values. In Figure 13b, in which the motion along X-axis is performed, the mean value of the error of the sensed vs. theoretical tilt angle is 1.5°, achieving values of less than 1° in the central zones. On the contrary, as we move away from the central zone of the workspace, this angle increases considerably. Similarly, in relation to the motion along Y-axis (Figure 14b), the mean error is 3.45°, achieving values up to 1.5° in

the central part. These results agree with the workspace plot shown in Figure 7, in which a quasi-translational motion is expected when the manipulator moves in and near the central zone. Therefore, this prototype serves as a proof of concept of the proposed model.

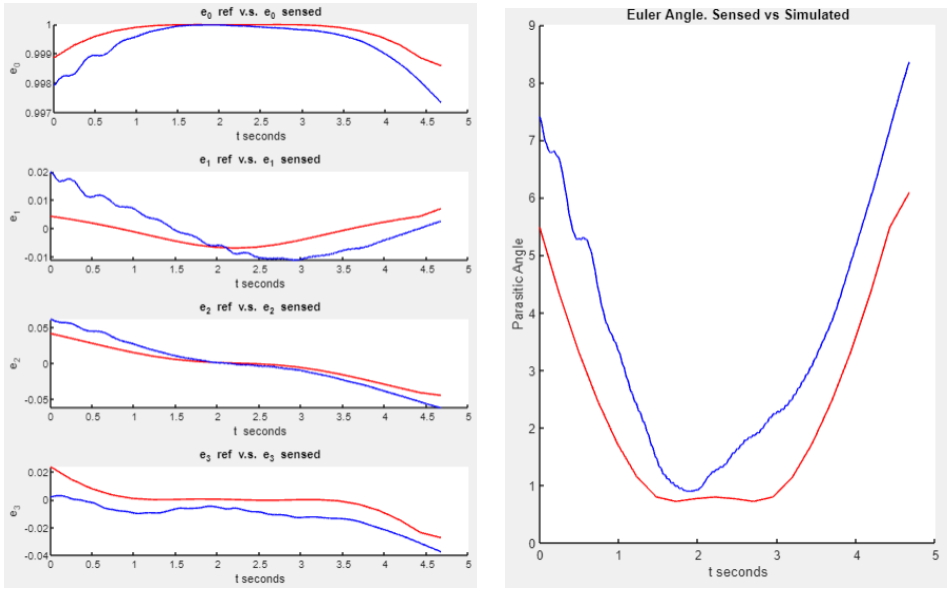

(**a**) (**b**)

Figure 13. Motion along X-axis: Theoretical (red) vs. Sensed (blue); (**a**) Quaternions; (**b**) Euler angle.

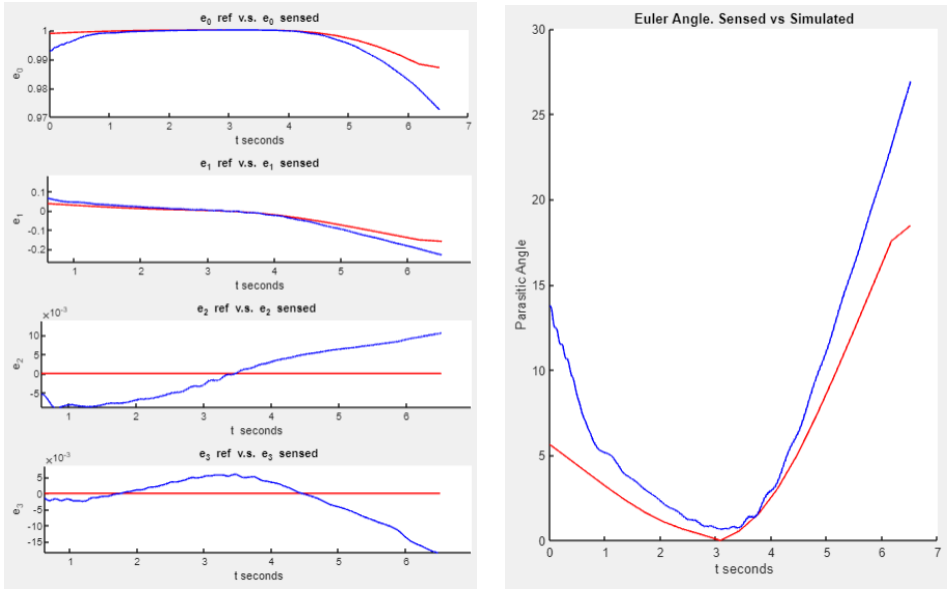

(**a**) (**b**)

Figure 14. Motion along Y-axis: Theoretical (red) vs. Sensed (blue); (**a**) Quaternions; (**b**) Euler angle.

We have included Supplementary Video files showing both the simulations in MATLAB R2023b and the corresponding motion of the Keops-Delta prototype during the experimental tests. We encourage the reader to view the attached multimedia material.

4. Discussion

In this work, the kinematic characterization of novel Delta type continuum parallel manipulators has been presented, obtaining the operational workspaces of the rotational Delta and Keops-Delta type flexible manipulators. It has been shown that, due to the inherent

flexibility of these continuum manipulators, the generated motion is not purely translational, as it happens in their rigid counterparts, but the central zones of the workspace present quasi-translational motions, while as we move away from this zone, the parasitic inclination angle of the moving platform increases progressively. The influence of the application of an external load on the moving platform on the resulting workspace has also been evaluated. The ability of these manipulators to withstand a vertical load of a similar value to that of equivalent Delta rigid robots has been demonstrated, provided that the load is applied in the vertical direction, or that the resulting combination of loads keeps the starting position as horizontal as possible.

In order to validate the proposed design, a prototype of the flexible Keops-Delta has been built, which incorporates superelastic Nitinol slender rods in the three parallelograms that make up its kinematic chains. The programming associated with the kinematic analysis has been implemented in a MATLAB GUI, which has also incorporated the experimental measurements performed with a MTi-680 sensor placed on the end-effector, in order to compare the theoretical results in relation to the inclination of the moving platform with the real measurements obtained in the experimental tests. It has been verified that, although there is a small difference between the theoretical values and the sensor measurements, the theoretical and real curves follow exactly the same trend, and furthermore demonstrate the capacity of the flexible Keops-Delta to generate quasi-translational motion in the central zones of the workspace.

As for future work, it could be interesting to implement a mechanical vibration damping approach in order to minimize the vibratory motions generated in the end-effector, mainly due to the flexibility of the slender rods.

Supplementary Materials: The following supporting information can be downloaded at: https://www.mdpi.com/article/10.3390/app14219744/s1. The videos referred to in the paper showing the simulations and real motions of the flexible Keops-Delta prototype are available.

Author Contributions: Conceptualization, O.A. and M.U.; methodology, O.A., M.U. and A.H.; software, O.A. and M.U.; validation, O.A., M.U., A.H. and E.A.; formal analysis, A.H.; investigation, O.A., M.U., A.H. and E.A.; resources, O.A. and M.U.; data curation, O.A. and M.U.; writing—original draft preparation, O.A. and M.U.; writing—review and editing, A.H. and E.A.; visualization, O.A., M.U., A.H. and E.A.; supervision, M.U. and A.H.; project administration, O.A. and A.H.; funding acquisition, O.A. All authors have read and agreed to the published version of the manuscript.

Funding: The authors wish to acknowledge the financial support received from the Spanish Government through the Ministerio de Ciencia e Innovación (Project PID2020-116176GB-I00) financed by MCIN/AEI/10.13039/501100011033 and the support for the research group through Project IT1480-22 provided by the Departamento de Educación from the Regional Basque Government.

Institutional Review Board Statement: Not applicable.

Informed Consent Statement: Not applicable.

Data Availability Statement: The original contributions presented in the study are included in the article/supplementary material, further inquiries can be directed to the corresponding author.

Conflicts of Interest: The authors declare no conflicts of interest.

References

1. Bryson, C.E.; Rucker, D.C. Toward parallel continuum manipulators. In Proceedings of the 2014 IEEE International Conference on Robotics and Automation (ICRA), Hong Kong, China, 31 May–7 June 2014; pp. 778–785.
2. Seriani, S.; Gallina, P.; Scalera, L.; Lughi, V. Development of n-DoF Preloaded Structures for Impact Mitigation in Cobots. *J. Mech. Robot.* **2018**, *5*, 051009. https://doi.org/10.1115/1.4040632.
3. Hüsing, E.; Weidemann, C.; Lorenz, M.; Corves, B.; Hüsing, M. Determining Robotic Assistance for Inclusive Workplaces for People with Disabilities. *Robotics* **2021**, *10*, 44. https://doi.org/10.3390/robotics10010044.
4. Iwatsuki, N.; Sawada, E.; Igarashi, J.; Ikeda, I. Motion Analysis and Control of a Flexible Spatial Closed-Loop Mechanism Made of a Certain Thin Elastic Plate. In Proceedings of the IFToMM WC2023, MMS 148, Tokyo, Japan, 5–10 November 2023, pp. 139–148. https://doi.org/10.1007/978-3-031-45770-8_14.

5. Howell, L.L. *Compliant Mechanisms*; John Wiley & Sons: Hoboken, NJ, USA, 2002.
6. McClintock, H.; Temel, F.Z.; Doshi, N.; Koh, J.s.; Wood, R.J. The milliDelta: A high-bandwidth, high-precision, millimeter-scale Delta robot. *Sci. Robot.* **2018**, *3*, eaar3018. https://doi.org/10.1126/scirobotics.aar3018.
7. Black, C.B.; Till, J.; Rucker, D.C. Parallel Continuum Robots: Modeling, Analysis, and Actuation-Based Force Sensing. *IEEE Trans. Robot.* **2018**, *34*, 29–47. https://doi.org/10.1109/TRO.2017.2753829.
8. Rucker, D.C.; III, R.J.W. Statics and Dynamics of Continuum Robots With General Tendon Routing and External Loading. *IEEE Trans. Robot.* **2011**, *27*, 1033–1044. https://doi.org/10.1109/TRO.2011.2160469.
9. Till, J.; Bryson, C.E.; Chung, S.; Orekhov, A.; Rucker, D.C. Efficient computation of multiple coupled Cosserat rod models for real-time simulation and control of parallel continuum manipulators. In Proceedings of the 2015 IEEE International Conference on Robotics and Automation (ICRA), Seattle, WA, USA, 26–30 May 2015; pp. 5067–5074. https://doi.org/10.1109/ICRA.2015.7139904.
10. Orekhov, A.L.; Aloi, V.A.; Rucker, D.C. Modeling parallel continuum robots with general intermediate constraints. In Proceedings of the 2017 IEEE International Conference on Robotics and Automation (ICRA), Singapore, 29 May–3 June 2017; pp. 6142–6149. https://doi.org/10.1109/ICRA.2017.7989728.
11. Till, J.; Rucker, D.C. Elastic Stability of Cosserat Rods and Parallel Continuum Robots. *IEEE Trans. Robot.* **2017**, *33*, 718–733. https://doi.org/10.1109/TRO.2017.2664879.
12. Zaccaria, F.; Idá, E.; Briot, S. A Boundary Computation Algorithm for the Workspace Evaluation of Continuum Parallel Robots. *ASME. J. Mech. Robot.* **2023**, *16*, 041010. https://doi.org/10.1115/1.4062585.
13. Laribi, M.; Romdhane, L.; Zeghloul, S. Analysis and dimensional synthesis of the DELTA robot for a prescribed workspace. *Mech. Mach. Theory* **2007**, *42*, 859–870. https://doi.org/10.1016/j.mechmachtheory.2006.06.012.
14. Stock, M.; Miller, K. Optimal Kinematic Design of Spatial Parallel Manipulators: Application to Linear Delta Robot. *J. Mech. Des.* **2003**, *125*, 292–301. https://doi.org/10.1115/1.1563632.
15. Vischer, P.; Clavel, R. Kinematic calibration of the parallel Delta robot. *Robotica* **1998**, *16*, 207–218. https://doi.org/10.1017/S0263574798000538.
16. Mirz, C.; Hüsing, M.; Takeda, Y.; Corves, B. Active Dynamic Balancing of Delta Robots in pick-and-place Tasks. In *Advances in Mechanism and Machine Science*; Okada, M., Ed.; Springer Nature: Cham, Switzerland, 2023; pp. 255–265.
17. Cheng, H.; Li, W. Reducing the Frame Vibration of Delta Robot in pick-and-place Application: An Acceleration Profile Optimization Approach. *Shock Vib.* **2018**, *2018*, 2945314. https://doi.org/10.1155/2018/2945314.
18. Weber, A. Delta Robots Feed the Need for Speed. *Assembly* **2015**, *58*, 28–31.
19. Wang, Y.; Liu, J.; Guo, M.; Wang, L. Research on the printing error of tilted vertical beams in delta-robot 3D printers. *Rapid Prototyp. J.* **2021**, *9*, 051009. https://doi.org/10.1108/RPJ-03-2020-0052.
20. Mitsantisuk, C.; Stapornchaisit, S.; Niramitvasu, N.; Ohishi, K. Force sensorless control with 3D workspace analysis for haptic devices based on delta robot. In Proceedings of the IECON 2015—41st Annual Conference of the IEEE Industrial Electronics Society, Yokohama, Japan, 9–12 November 2015; pp. 001747–001752. https://doi.org/10.1109/IECON.2015.7392354.
21. Merlet, J. *Parallel Robots*; Springer: Cham, Switzerland, 2006. https://doi.org/10.1007/1-4020-4133-0.
22. Hüsing, M.; Weidemann, C.; Keunecke, S.C.; Hüsing, E.; Youness-Sinaky, R.; Jansen, C. IIDEA Project, RWTH Aachen University. 2024. Available online: https://www.iidea.rwth-aachen.de (accessed on 16 September 2024).
23. Mandischer, N.; Gürtler, M.; Weidemann, C.; Hüsing, E.; Bezrucav, S.O.; Gossen, D.; Brünjes, V.; Hüsing, M.; Corves, B. Toward Adaptive Human–Robot Collaboration for the Inclusion of People with Disabilities in Manual Labor Tasks. *Electronics* **2023**, *12*, 1118. https://doi.org/10.3390/electronics12051118.
24. IGUS. Drylin Robot Delta. 2024. Available online: https://www.igus.es/product/20437?artNr=DLE-DR-0050 (accessed on 1 October 2024).
25. Wu, G.; Shi, G. Experimental statics calibration of a multi-constraint parallel continuum robot. *Mech. Mach. Theory* **2019**, *136*, 72–85. https://doi.org/10.1016/j.mechmachtheory.2019.02.013.
26. Yang, Z.; Zhu, X.; Xu, K. Continuum Delta Robot: A Novel Translational Parallel Robot with Continuum Joints. In Proceedings of the 2018 IEEE/ASME International Conference on Advanced Intelligent Mechatronics (AIM), Auckland, New Zealand, 9–12 July 2018; pp. 748–755. https://doi.org/10.1109/AIM.2018.8452695.
27. Böttcher, G.; Lilge, S.; Burgner-Kahrs, J. Design of a Reconfigurable Parallel Continuum Robot with Tendon-Actuated Kinematic Chains. *IEEE Robot. Autom. Lett.* **2021**, *6*, 1272–1279. https://doi.org/10.1109/LRA.2021.3057557.
28. Lilge, S.; Burgner-Kahrs, J. Kinetostatic Modeling of Tendon-Driven Parallel Continuum Robots. *IEEE Trans. Robot.* **2023**, *39*, 1563–1579. https://doi.org/10.1109/TRO.2022.3226157.
29. Maraje, S.; Nurahmi, L.; Caro, S. Operation Modes Comparison of a Reconfigurable 3-PRS Parallel Manipulator Based on Kinematic Performance. In Proceedings of the International Design Engineering Technical Conferences and Computers and Information in Engineering Conference: 40th Mechanisms and Robotics Conference, Charlotte, NC, USA, 21–24 August 2016. https://doi.org/10.1115/DETC2016-59804.
30. Nurahmi, L.; Caro, S.; Wenger, P. Operation Modes and Singularities of 3-PRS Parallel Manipulators with Different Arrangements of P-Joints. In Proceedings of the International Design Engineering Technical Conferences and Computers and Information in Engineering Conference: 39th Mechanisms and Robotics Conference, Boston, MA, USA, 2–5 August 2015. https://doi.org/10.1115/DETC2015-47935.

31. Altuzarra, O.; Tagliavini, L.; Lei, Y.; Petuya, V.; Ruiz-Erezuma, J.L. On Constraints and Parasitic Motions of a Tripod Parallel Continuum Manipulator. *Machines* **2023**, *11*, 71. https://doi.org/10.3390/machines11010071.
32. Holst, G.L.; Teichert, G.H.; Jensen, B.D. Modeling and Experiments of Buckling Modes and Deflection of Fixed-Guided Beams in Compliant Mechanisms. *J. Mech. Des.* **2011**, *133*, 051002. https://doi.org/10.1115/1.4003922.
33. Altuzarra, O.; Caballero, D.; Campa, F.J.; Pinto, C. Position analysis in planar parallel continuum mechanisms. *Mech. Mach. Theory* **2019**, *132*, 13–29. https://doi.org/10.1016/j.mechmachtheory.2018.10.014.
34. Altuzarra, O.; Merlet, J.P. Certified Kinematics Solution of 2-DOF Planar Parallel Continuum Mechanisms. In *Advances in Mechanism and Machine Science*; Uhl, T., Ed.; Springer International Publishing: Cham, Switzerland, 2019; pp. 197–208.
35. Altuzarra, O.; Urizar, M.; Cichella, M.; Petuya, V. Kinematic Analysis of three degrees of freedom planar parallel continuum mechanisms. *Mech. Mach. Theory* **2023**, *185*, 105311. https://doi.org/10.1016/j.mechmachtheory.2023.105311.
36. Duan, X.; Yan, W.; Chen, G.; Wang, H. Analysis and validation of a planar parallel continuum manipulator with variable Cartesian stiffness. *Mech. Mach. Theory* **2022**, *177*, 105030. https://doi.org/10.1016/j.mechmachtheory.2022.105030.
37. Chen, G.; Kang, Y.; Liang, Z.; Zhang, Z.; Wang, H. Kinetostatics modeling and analysis of parallel continuum manipulators. *Mech. Mach. Theory* **2021**, *163*, 104380. https://doi.org/10.1016/j.mechmachtheory.2021.104380.
38. Briot, S.; Boyer, F. A Geometrically Exact Assumed Strain Modes Approach for the Geometrico- and Kinemato-Static Modelings of Continuum Parallel Robots. *IEEE Trans. Robot.* **2023**, *39*, 1527–1543. https://doi.org/10.1109/TRO.2022.3219777.
39. Lang, H.; Linn, J.; Arnold, M. Multi-body dynamics simulation of geometrically exact Cosserat rods. *Multibody Syst. Dyn.* **2011**, *25*, 285–312. https://doi.org/10.1007/s11044-010-9223-x.
40. Bouri, M.; Clavel, R. The Linear Delta: Developments and Applications. In Proceedings of the Robotics (ISR), 2010 41st International Symposium on and 2010 6th German Conference on Robotics (ROBOTIK), Munich, Germany, 7–9 June 2010; pp. 1–8.
41. Briot, S.; Goldsztejn, A. Singularity Conditions for Continuum Parallel Robots. *IEEE Trans. Robot.* **2022**, *38*, 507–525. https://doi.org/10.1109/TRO.2021.3076830.
42. Zaccaria, F.; Idá, E.; Briot, S.; Carricato, M. Workspace Computation of Planar Continuum Parallel Robots. *IEEE Robot. Autom. Lett.* **2022**, *7*, 2700–2707. https://doi.org/10.1109/LRA.2022.3143285.

Disclaimer/Publisher's Note: The statements, opinions and data contained in all publications are solely those of the individual author(s) and contributor(s) and not of MDPI and/or the editor(s). MDPI and/or the editor(s) disclaim responsibility for any injury to people or property resulting from any ideas, methods, instructions or products referred to in the content.